HHS Public Access

Author manuscript

Invest Radiol. Author manuscript; available in PMC 2024 October 21.

Published in final edited form as:

Invest Radiol. 2022 August 01; 57(8): 495–501. doi:10.1097/RLI.0000000000000864.

Cone-beam CT-based spatial prediction of drug dose following transarterial chemoembolization using radiopaque drug-eluting beads in woodchuck hepatocellular carcinoma

Andrew S. Mikhail, PhD,
Center for Interventional Oncology, Radiology and Imaging Sciences, Clinical Center, National Institutes of Health, Bethesda, MD, USA

William F. Pritchard, MD, PhD,
Center for Interventional Oncology, Radiology and Imaging Sciences, Clinical Center, National Institutes of Health, Bethesda, MD, USA

Ayele H. Negussie, PhD,
Center for Interventional Oncology, Radiology and Imaging Sciences, Clinical Center, National Institutes of Health, Bethesda, MD, USA

Gazi Inkiyad, BSc,
Biomedical Engineering Summer Internship Program, Center for Interventional Oncology, Radiology and Imaging Sciences, Clinical Center, National Institutes of Health, Bethesda, MD, USA

Dilara J. Long, BA,
Center for Interventional Oncology, Radiology and Imaging Sciences, Clinical Center, National Institutes of Health, Bethesda, MD, USA

Michal Mauda-Havakuk, MD, PhD,
Center for Interventional Oncology, Radiology and Imaging Sciences, Clinical Center, and the National Institute of Biomedical Imaging and Bioengineering; National Institutes of Health, Bethesda, MD, USA

Paul G. Wakim, PhD,
Biostatistics and Clinical Epidemiology Service, Clinical Center, National Institutes of Health, Bethesda, MD, USA

William van der Sterren, MSc,
IGT Systems Innovation, Philips, Best, The Netherlands

Elliot B. Levy, MD,
Center for Interventional Oncology, Radiology and Imaging Sciences, Clinical Center, National Institutes of Health, Bethesda, MD, USA

Andrew L. Lewis, PhD,
Owen Mumford Ltd. Woodstock, Oxfordshire, GB

Address correspondence to: Andrew S. Mikhail, Clinical Center, Room 3N320A, MSC 1182, National Institutes of Health, 10 Center Drive, Bethesda, MD, USA, 20892, andrew.mikhail@nih.gov.

John W. Karanian, PhD,
Center for Interventional Oncology, Radiology and Imaging Sciences, Clinical Center, National Institutes of Health, Bethesda, MD, USA

Bradford J. Wood, MD
Center for Interventional Oncology and Chief, Interventional Radiology, National Cancer Institute Center for Cancer Research and Radiology and Imaging Sciences, Clinical Center, National Institutes of Health, Bethesda, MD, USA

Abstract

Objectives: To develop a model to estimate drug dose delivered to tumors following transarterial chemoembolization (TACE) with radiopaque drug-eluting beads (DEB) based on DEB density on cone-beam computed tomography (cone-beam CT) and to evaluate drug penetration into tissue in a woodchuck hepatoma model.

Materials and Methods: TACE was performed in woodchucks with hepatocellular carcinoma (N=5) using DEB (70-150 μm, LC Bead LUMI) loaded with doxorubicin. Livers were resected 45 minutes after embolization, immediately frozen, and cut using liver-specific, 3D-printed sectioning molds. Doxorubicin levels in tumor specimens were measured by high performance liquid chromatography (HPLC) and correlated with DEB iodine content that was measured using prototype cone-beam CT-based embolization treatment planning software. Doxorubicin penetration into tissue surrounding DEB was assessed by fluorescence microscopy of tumor sections. Fluorescence intensity was converted into doxorubicin concentration using calibration standards. Intensity-thresholded color heatmaps were generated representing extravascular drug penetration.

Results: Consistent segmentation of DEB on cone-beam CT was achieved using a semi-automated intensity thresholding method. A positive linear correlation (0.96) was found between DEB iodine content measured on cone-beam CT and the amount of doxorubicin measured in tumor specimens. Prediction of doxorubicin levels in tumor sections that were not included in model development was accurate with a root mean square error of 0.08 mg of doxorubicin. Tumor penetration of eluted doxorubicin resulted in concentration gradients where drug content decreased with increasing distance from blood vessels containing DEB. Drug penetration was greater for blood vessels containing DEB clusters compared to single DEB, with higher doxorubicin concentrations extending further away from the vessels.

Conclusions: Estimation of drug dose delivered during TACE in a woodchuck hepatocellular carcinoma model was possible using DEB radiopacity on cone-beam CT as a surrogate marker. Doxorubicin penetration was greatest adjacent to vessels containing DEB clusters compared to single DEB. Intra-procedural estimation of the spatial distribution of drug dose within the tumor could enable real-time adjustments to DEB delivery, in order to maximize treatment coverage or identify regions of tumor at risk for undertreatment.

Keywords

drug-eluting beads; image-guided drug delivery; embolization; microspheres; spatial drug dosimetry; cancer; doxorubicin; DEB-TACE; drug penetration; cone-beam computed tomography

Introduction

Transarterial chemoembolization (TACE) is a minimally invasive procedure performed with chemotherapy and embolic material to treat hepatic malignancies. Drug-eluting beads (DEB) containing doxorubicin are used for TACE (DEB-TACE) both as an embolic and drug delivery system resulting in sustained local-regional delivery of chemotherapy and limited systemic drug exposure.[1-4] However, variability in DEB-TACE treatment parameters, including type and size of DEB, drug, and treatment endpoints has contributed to a lack of standardization and reproducibility. Refinement of DEB-TACE techniques may benefit from direct intra-procedural visual feedback regarding treatment localization, including distribution of both embolic material and eluted drug, and ultimately spatial prediction of therapeutic effects.

Assessments of DEB-TACE completion and adequacy generally rely on transient patterns of retained soluble contrast at immediate post-procedural imaging, without direct visualization of DEB location.[5-9] However, the development of iodinated DEB with inherent radiopacity has enabled visual feedback regarding spatial distribution of DEB on cone-beam CT, CT or fluoroscopy.[10-12] Delineation of DEB localization in relation to enhancing tumor may be achieved by fusion or subtraction of cone-beam CT or CT images, which enables identification of residual tumor tissue at risk for undertreatment.[13] Recently, the image-ability of radiopaque DEB on CT was shown to act as a surrogate marker of drug distribution potentially enabling spatial drug dosimetry.[14] The ability to estimate and map the spatial distribution of drug dose on imaging could improve treatment uniformity and may provide insight into the relative contributions of drug effects and ischemia towards treatment efficacy.

It has been previously demonstrated that attenuation and volume of radiopaque DEB measured on CT are proportional to drug dose following embolization using a rabbit VX2 preclinical model, permitting accurate prediction of drug dose in the liver.[14] In the present study, the concept of drug dose mapping was applied to cone-beam CT to explore the potential for intra-procedural assessment and iterative guidance of drug delivery. Iodine content on cone-beam CT was measured using prototype segmentation and iodine quantification software and correlated with doxorubicin levels in a woodchuck hepatic tumor model that has vascularization and imaging characteristics comparable to human hepatocellular carcinoma (HCC).[15, 16] Woodchucks bearing hepatic tumors arising from chronic infection with woodchuck hepatitis virus are useful models for studying catheter-based therapies of HCC.[15, 17, 18] The purpose of our study was to evaluate iodine content on cone-beam CT as a surrogate marker for spatial drug delivery following embolization with drug-eluting radiopaque DEB using an investigational prototype segmentation software tool and to evaluate extravascular drug penetration in a woodchuck HCC model.

Materials and Methods

Animal Model

This study was conducted under an animal use protocol approved by the institutional animal care and use committee in compliance with US Animal Welfare Regulations.

Five woodchucks (Marmota monax) (Northeastern Wildlife, Harrison, Idaho, USA) were studied: three males and two females (average weight = 3.88 kg, range 2.5-4.9). Each was chronically infected with woodchuck hepatitis virus following inoculation within the first week of life and confirmed as tumor-positive by the vendor based on serum γ-glutamyl transpeptidase levels greater than 50 IU/L prior to our acquisition of the animals.[19] Woodchucks were individually housed with 12-hour light:dark cycling, ad libitum access to food and water, and environmental enrichment. Cage-side observations were performed twice-daily.

Chemoembolization with Radiopaque DEB

Chemoembolization was performed as previously described.[15] Woodchucks with HCC tumors were anesthetized and the femoral artery was surgically exposed and cannulated using a 3-F introducer sheath (Cook, Inc., Bloomington, Indiana). Selective hepatic arterial catheterization was performed using a 2.0-F microcatheter (Excelsior 1018; Stryker Neurovascular, Fremont, California) or 2.4-F microcatheter (Progreat Microcatheter System [Terumo, Somerset, New Jersey] or 2.8-F tapered to 2.1-F Merit Maestro Microcatheter [Merit Medical, South Jordan, Utah]) under fluoroscopic guidance (Allura Xper FD20; Philips, Best, the Netherlands). Doxorubicin had been preloaded into radiopaque DEB (70-150 μm, LC Bead LUMI, Biocompatibles UK Ltd, Farnham, UK, now Boston Scientific, Marlborough, MA) at a concentration of 37.5 mg/mL sedimented wet DEB. The use of doxorubicin with radiopaque DEB is investigational. Radiopaque DEB were suspended in iohexol contrast media (Omnipaque 350, GE Healthcare AS, Oslo, Norway) at a dilution of 1 part DEB to 9 parts 100% iohexol. Suspended DEB were injected slowly with gentle inversion of the syringe to avoid clumping until blood flow stasis and woodchucks were euthanized (Euthasol 1 mL/10lb; Virbac Animal Health, Fort Worth, TX) forty-five minutes later. Whole livers were resected and immediately placed in a freezer at −80°C.

Preparation of Tissue Samples

Subject-specific, 3D-printed cutting molds were used to aid the sectioning of frozen livers and tumors into parallel samples of consistent thickness (5 mm), as previously reported.[14, 20] Briefly, woodchuck livers or tumors were explanted, frozen at −80°C, and a cone-beam CT (Allura Xper FD-20; Philips, Best, The Netherlands) was acquired of each specimen. To create the cutting molds, image segmentation was performed using Mimics Research software package (version 20.0; Materialise, Leuven, Belgium) and a virtual 3D model of the liver or tumor was created. The model was imported into computer-aided design software (Solidworks, Waltham, MA) and subtracted from a rectangular block designed with cutting slots spaced 5 mm apart. This virtual 3D cutting mold, containing the liver or tumor-shaped cavity, was divided into two halves and each was printed on a 3D printer (uPrint Plus, Stratasys, Eden Prairie, MN). Whole frozen livers or tumors were inserted into the mold and a fine saw was passed through the cutting slots. Tumor samples 5 mm in thickness were removed from the mold and subdivided into 2-3 pieces such that they measured approximately 2 x 2 x 0.5 cm. A cone-beam CT scan of samples comprised entirely of tumor (n = 44) was acquired using a 100 kVp scan protocol (Philips) specifically designed for radiopaque DEB. Micro-CT (Quantum GX; Perkin Elmer, Waltham, Mass) was acquired for selected sections at 90 kVp. Additional frozen tumor samples (n = 11) were cut

using a cryostat with thickness of 10 μm, mounted on a microscope slide, and stained with hematoxylin and eosin for histopathology or left unstained for analysis of doxorubicin tissue penetration.

Measurement of Iodine on Cone-beam CT

An investigational prototype segmentation software tool (Emboguide, Philips, Best, the Netherlands) was used that measured the increase in radiographic density in Hounsfield units (HU) above a reference value measured in untreated liver in a cone-beam CT scan of tumor samples. The software then converted HU to milligrams of iodine in a region of interest (ROI) encompassing a tumor sample. The software automatically performed DEB segmentations within the target ROI using an intensity threshold equal to twice the standard deviation of the mean voxel intensity within the manually-selected reference region using the following equation:

$$HU_{threshold} = mean\ HU_{reference} + 2\ \sigma_{reference}$$

where HU is the x-ray attenuation in Hounsfield units and $\sigma_{reference}$ is the standard deviation of the mean x-ray attenuation in the reference region. Voxels with HU greater than $HU_{threshold}$ were included in the segmented region. The software was calibrated by the manufacturer to convert x-ray attenuation in HU to iodine concentration by acquiring cone-beam CT scans of solutions of known iodine concentration at 120 kVp. Using this conversion factor (1 mg iodine/mL per 23 HU), the difference between the HU of each voxel within the segmented region and the threshold HU was automatically converted to milligrams of iodine using the following equation:

$$Iodine\,(mg) = \sum [(HU_{segmented\,voxel} - HU_{threshold}) \times \frac{1\frac{mg\,iodine}{mL}}{23\,HU} \times voxel\ volume]$$

where the total iodine content was the sum of iodine for all pixels contained within the segmented region. We performed a similar calibration by imaging iohexol solutions (Omnipaque 350, GE Healthcare, Oslo, Norway) at known concentrations to determine the correlation between HU and iodine concentration at 100 kVp using the 100 kVp cone-beam CT protocol. The ratio of the HU-iodine conversion factors at 120 kVp and 100 kVp (1 mg iodine/mL per 46.5 HU, see supplemental figure S1) was used as a post hoc correction factor for the iodine measurements based on cone-beam CT scans acquired at 100 kVp, since radiopaque DEB detection is greater with the 100 kVp scan than at 120 kVp.[21]

Radiopaque DEB were suspended in agarose gel phantoms (1 mL agarose, 0.5% [vol/vol])) at five DEB concentrations (0.78-12.5% [vol DEB/vol agarose]). A cone-beam CT scan at 100 kVp was acquired of the agarose phantoms with DEB as well as agarose without DEB and of embolized tumor sections and unembolized sections of liver parenchyma. Reference regions were manually selected within the blank agarose phantoms or unembolized liver sections. Target regions of interest were selected that were comprised of individual DEB phantoms or the entirety of embolized tumor sections.

Quantification of Doxorubicin

Doxorubicin was extracted from DEB phantoms or tumor samples and quantified following a previously described procedure.[14] Briefly, DEB phantoms or tumor samples were repeatedly homogenized in a solution of acetonitrile, water, and potassium chloride (3:10:1, v:v:g) using a Bead Ruptor homogenizer (OMNI International, Kennesaw, GA). Following centrifugation, 25 μL of supernatant from each sample was diluted in 0.9 mL potassium phosphate (pH 3.8). Daunorubicin (100 μL, 2.5 mg/mL in water) was added as an internal standard and each solution was incubated at 37°C for 15 min. Acetone (250 μL) and a saturated solution of zinc sulfate (100 μL) were then added to each vial and incubated at 37°C for 15 min. Samples of supernatant (0.5 mL) were transferred to vials and dried. The dried residues were dissolved completely in the HPLC mobile phase and transferred to HPLC vials. Doxorubicin concentration in the samples was determined by comparison of elution peaks to samples of known concentration using a Zobrax Eclipse Plus C18 reversed-phase column (Agilent, Santa Clara, CA) connected to a fluorescence detector. The mobile phase consisted of 0.1% trifluoroacetic acid in acetonitrile and deionized water (34:66) at a flow rate of 1.5 mL/min at 30°C with an injection volume of 5 μL.

Doxorubicin heatmaps and extravascular tumor penetration

Doxorubicin tissue distribution was assessed in unstained slide-mounted tumor sections (n=6) from three woodchucks using a fluorescence microscope (Axio Imager.M1; Zeiss, Thornwood, NY) with a 10X objective (pixel size, 0.64 μm; binning, 2 X 2). Images were captured using a monochrome charge-coupled device camera, motorized scanning stage, and Zen imaging software (Zeiss). Segmentations of DEB and doxorubicin in tumors were performed using MATLAB's Image Processing Toolbox (MathWorks, Natick, Mass). Masks of tissue, i.e., extravascular regions, and DEB were generated by intensity thresholding (Figure 1). Doxorubicin heatmaps were generated using intensity thresholds equal to the mean pixel intensity of untreated tumor sections plus multiples of the standard deviation, from two to five, in increments of 0.5. Pixels were grouped into "bins" defined by the intensity thresholds and pseudo-colored, from blue to red, indicating low and high concentrations of doxorubicin, respectively. Calibration standards were created by applying doxorubicin solutions with known concentrations to untreated liver sections enabling conversion of pixel intensity to doxorubicin concentration. Pixels associated with DEB masks were pseudo-colored white for the purpose of visualization and were excluded from the image for the heatmap analysis.

Semiquantitative analysis of doxorubicin extravascular tissue penetration was performed by measuring the fluorescence intensity and distance of doxorubicin -positive pixels from tumor blood vessel margins (n = 17). Blood vessels containing DEB were manually contoured and the average fluorescence intensity was calculated by randomly sampling 500 pixels from each 1-pixel-thick concentric band up to 600 μm from the blood vessel. Intensity values were converted to doxorubicin concentration as described above. Tumor tissue penetration of eluted doxorubicin was expressed as a function of distance from DEB for single DEB and from clusters containing 2 or more DEB (where the median cluster size was 6.5 DEB). Selected slides were counterstained with TO-PRO-3 (Invitrogen, Carlsbad, CA) for visualization of cell nuclei. Two independent channels were captured: Cy5 for nuclei (blue)

and a custom filter cube (excitation, 480/40 nm; emission, 600/60 nm) corresponding to excitation and emission spectra of doxorubicin (red).

Statistical Modeling and Predicting DOX Concentration

Predictions of doxorubicin content in embolized tumors were based on statistical models correlating the amount of doxorubicin measured in tumor samples with iodine content measured on cone-beam CT. Repeated measures analyses, mixed models, that account for intra- and inter-subject correlations were used to estimate model parameters, where the subjects were the individual woodchucks. Based on doxorubicin content predictions from these models, the average, median, minimum, and maximum residuals, the difference between the actual measurement value and the predicted value, as well as the root mean square error were determined to assess the models' predictive power. The analyses were performed by using data collected from five woodchucks. Additional analyses were performed by using data from four of the five woodchucks to predict doxorubicin content in the fifth woodchuck. This leave-one-out method was repeated five times, excluding a different woodchuck each time.

Results

Correlation of Iodine with Attenuation and Doxorubicin in vitro

Attenuation measured on cone-beam CT correlated linearly with iodine content in iohexol solutions (Supplemental figure S1). Doxorubicin measured in DEB phantoms was linearly proportional to iodine content measured on cone-beam CT (slope = 0.35; CI: 0.33-0.37), using the iodine-HU correlation (Figure 2).

Radiopaque DEB Conspicuity

Cone-beam CT of liver explants revealed readily conspicuous radiopaque DEB within tortuous blood vessels inside highly vascular tumors (Figure 3 A). Some regions containing DEB in low densities could not be visualized on cone-beam CT but were conspicuous on microCT (Figure 3 B, C). All embolized tumors used for analysis of DEB conspicuity and drug extraction (n=5) were confirmed to be HCC at histopathologic examination.

Extravascular Penetration of Doxorubicin

Fluorescence microscopy of tumor sections showed DEB in tumor blood vessels surrounded by doxorubicin that had eluted into surrounding tissue (Figure 4 A). Eluted doxorubicin decreased in intensity with increasing distance from the DEB (Figure 4 B). Doxorubicin penetration was greater adjacent to vessels containing DEB clusters compared to single DEB, with higher concentrations observed up to 600 μm away from DEB. Heterogeneous distribution of DEB and co-localized doxorubicin was apparent within tumor sections (Figure 5).

Prediction of Doxorubicin Concentration in Tumor

The amount of doxorubicin measured in tumor samples collected 45 minutes after DEB-TACE correlated linearly with the amount of iodine measured on cone-beam CT (slope =

0.13, CI: 0.09-0.17) (Figure 6 A). Iodine was a strong predictor of doxorubicin content in the tumors with a root mean square error of 0.08 mg of doxorubicin (Table 1). Predicted doxorubicin levels based on cone-beam CT images were accurate when compared to the actual amount of doxorubicin measured (Figure 6 B). The relative accuracy of model predictions is demonstrated by the proximity of the points in the plot to the identity line.

Discussion

Limited visual feedback regarding the spatial distribution of embolic and drug during DEB-TACE may contribute to the lack of treatment standardization and reproducibility. This study demonstrates the use of cone-beam CT imaging to estimate the amount of doxorubicin delivered to tumors following DEB-TACE with iodinated radiopaque DEB in a woodchuck HCC tumor model. We found that doxorubicin measured in tumor samples was proportional to the amount of iodine measured on cone-beam CT using prototype segmentation software. This correlation enabled accurate cone-beam CT-based predictions of drug dose in embolized tumors suggesting that intra-procedural estimation of drug distribution is feasible.

Radiopaque DEB contain permanently bound iodine within their structure that imparts radiodensity and enables real-time visualization of DEB spatial distribution on clinical imaging.[10-14] In this study, we developed a correlative model using clinical cone-beam CT and investigational software with the goal of facilitating immediate real-time intraprocedural iterative modifications in treatment. An investigational prototype segmentation software tool used a semi-automated thresholding algorithm to compare the attenuation in user-defined untreated reference regions in liver to the attenuation in treated target regions of embolized tumor samples. The software calculated the amount of iodine, which was proportional to x-ray attenuation, present in DEB phantoms and embolized tumors using cone-beam CT imaging.

The overarching goal of this study was to assess whether cone-beam CT could estimate spatial drug dose when using radiopaque DEB for DEB-TACE. Predictions of drug dose were conducted based on correlations of iodine measured on cone-beam CT with doxorubicin levels in tumor samples using a repeated-measures model. The strength of the correlation was found to be comparable to previous work in rabbit VX2 tumors using multidetector CT for measurement of DEB attenuation.[14] Compared to VX2 tumors, the woodchuck HCC model more closely recapitulates the tumor microenvironment and vascularity of human HCC. Model-based predictions were accurate when compared to actual doxorubicin measured in tumor samples suggesting that similar approaches could be used to predict drug dose and drug spatial distribution in patients undergoing DEB-TACE with radiopaque DEB using cone-beam CT. Iodine measured on cone-beam CT using this approach was found to be linearly proportional to the amount of doxorubicin measured in DEB phantoms and embolized tumor samples. Lower amounts of doxorubicin relative to iodine were found in tumor samples compared to DEB phantoms likely due to partial release of doxorubicin from DEB and subsequent clearance from the tumor in vivo. The presence of residual soluble contrast administered during tumor embolization may have also contributed

to the difference in the slopes of the doxorubicin versus iodine plots for tumor samples and DEB phantoms.

The relative colocalization of DEB and drug in tumor samples was consistent with previous findings demonstrating controlled elution of doxorubicin in vivo.[14, 22, 23] These findings support the concept of radiopaque DEB as a potential surrogate of drug delivery and spatial distribution. This is in contradistinction to ethiodized oil (standardly used in TACE), which dissociates rapidly from doxorubicin following administration making it a poor predictor of spatial drug levels.[24] Drug concentration heatmaps generated based on fluorescence imaging of tumor sections revealed partial doxorubicin elution from DEB into surrounding tissue 45 minutes after DEB-TACE. DEB were found in variably sized clusters spread heterogeneously throughout tumor sections and confined to the vascular compartment. Higher doxorubicin concentrations were apparent in tumor tissue surrounding DEB clusters compared to single DEB. While this study describes drug distribution relative to DEB at a single point in time, prior work indicates that drug distribution is dynamic.[22, 23] Further study is needed to define the relationship between radiopaque DEB and drug distribution over time.

This study demonstrates the use of cone-beam CT with integrated prototype software to quantify iodine after embolization with radiopaque DEB and predict corresponding drug levels in a translational tumor model. The ability to visualize DEB distribution, quantify iodine, and then predict drug spatial distribution and dose may facilitate evaluation of biological processes and pathways associated with treatment response temporally and spatially, and ultimately enable tools for predicting and improving outcomes.

This study had multiple limitations. Soluble contrast retained in the tumor following DEB-TACE may have affected the correlation of x-ray attenuation and doxorubicin levels. This effect was minimized by waiting 45 minutes for contrast to clear following completion of embolization before imaging and tissue collection. Also, very low DEB densities may be undetectable on clinical imaging, but the effect on drug dose estimation is unknown.[21] Drug levels in tumor samples were correlated with iodine levels measured using a cone-beam CT of frozen liver explants. Hounsfield unit values may differ slightly for cone beam CT of liver and radiopaque DEB in vivo. It is also important to note that the proportion of doxorubicin still located inside the DEB was not differentiated from free doxorubicin in tissue during quantitative analysis of doxorubicin in tumor samples. However, fluorescence imaging of tumor sections demonstrated partial drug elution and extravascular tumor penetration 45 min post embolization. In the future, more refined models of drug dose mapping might incorporate measures of DEB distribution, drug elution kinetics, tissue pharmacokinetics, and local tumoricidal dose thresholds in order to better predict therapeutic efficacy.

Conclusions

Spatial estimation of drug dose delivered during TACE was possible using DEB radiopacity on cone-beam CT as a drug surrogate in a woodchuck hepatocellular carcinoma model. This suggests that intra-procedural visualization with cone-beam CT, potentially fused with other imaging data, may estimate the magnitude and spatial distribution of drug dose within the

tumor. In future work, correlative models capturing the association between DEB density, distribution, and elution kinetics may also shed light on the relative contributions of drug and ischemia to therapeutic effects. This information may inform real-time adjustments to DEB delivery in order to maximize treatment coverage or identify regions of tumor at risk for undertreatment and could benefit procedural standardization, outcomes, and mechanistic understanding of DEB-TACE for HCC.

Supplementary Material

Refer to Web version on PubMed Central for supplementary material.

Conflicts of Interest and Source of Funding

This work was supported by the Center for Interventional Oncology in the Intramural Research Program of the National Institutes of Health (NIH) by intramural NIH Grants NIH Z01 1ZID BC011242 and CL040015. Dr. Mauda-Havakuk is supported by the Clinical Translational Fellowship Program of the NIH Clinical Center and the Intramural Research Program of the National Institute of Biomedical Imaging and Bioengineering. NIH has a Materials Transfer Agreement with Northeastern Wildlife. The NIH has Cooperative Research and Development Agreements with Biocompatibles UK Ltd-Boston Scientific Corporation and Philips that provide support for this research. NIH had control over the conduct of the study, the inclusion of any data, data analysis and interpretation, manuscript preparation and decisions on submission for publication. The content of this manuscript does not necessarily reflect the views or policies of the US Department of Health and Human Services. The mention of commercial products, their source, or their use in connection with material reported herein is not to be construed as an actual or implied endorsement of such products by the United States government.

William van der Sterren is an employee of Philips. Professor Andrew L Lewis was an employee of Biocompatibles UK Ltd, the company sponsoring the study. BJW is the Principal Investigator for Cooperative Research & Development Agreements between NIH and the following: BTG Biocompatibles/Boston Scientific, Siemens, Philips, NVIDIA, Celsion Corp, Canon Medical, XAct Robotics. BJW and NIH are party to Material Transfer or Collaboration Agreements with: Angiodynamics, 3T Technologies, Profound Medical, Exact Imaging, Johnson and Johnson, Endocare/Healthtronics, and Medtronic. Outside the submitted work, BJW is primary inventor on 47 issued patents owned by the NIH (list available upon request), a portion of which have been licensed by NIH to Philips. BJW and NIH report a licensing agreement with Canon Medical on algorithm software with no patent. BJW is joint inventor (assigned to HHS NIH US Government) for patents and pending patents related to drug-eluting bead technology, some of which have joint inventorships with BTG Biocompatibles/Boston Scientific. BJW is primary inventor on patents owned by NIH in the space of drug-eluting embolic beads. The authors report no other conflicts of interest in this work.

This manuscript discusses the use of an investigational device, software for iodine quantification in Emboguide, a Philips product.

References

1. Civalleri D, Esposito M, Fulco R, et al. Liver and tumor uptake and plasma pharmacokinetic of arterial cisplatin administered with and without starch microspheres in patients with liver metastases. Cancer. 1991;68:988–94. [PubMed: 1913493]
2. Varela M, Real MI, Burrel M, et al. Chemoembolization of hepatocellular carcinoma with drug eluting beads: efficacy and doxorubicin pharmacokinetics. J Hepatol. 2007;46:474–81. [PubMed: 17239480]
3. Poon RT, Tso WK, Pang RW, et al. A phase I/II trial of chemoembolization for hepatocellular carcinoma using a novel intra-arterial drug-eluting bead. Clin Gastroenterol Hepatol. 2007;5:1100–8. [PubMed: 17627902]
4. Mikhail AS, Negussie AH, Mauda-Havakuk M, et al. Drug-eluting embolic microspheres: State-of-the-art and emerging clinical applications. Expert Opin Drug Deliv. 2021;18:383–98. [PubMed: 33480306]

5. Golowa YS, Cynamon J, Reinus JF, et al. Value of noncontrast CT immediately after transarterial chemoembolization of hepatocellular carcinoma with drug-eluting beads. J Vasc Interv Radiol. 2012;23:1031–5. [PubMed: 22739645]
6. Suk Oh J, Jong Chun H, Gil Choi B, Giu Lee H. Transarterial chemoembolization with drug-eluting beads in hepatocellular carcinoma: Usefulness of contrast saturation features on cone-beam computed tomography imaging for predicting short-term tumor response. J Vasc Interv Radiol. 2013;24:483–9. [PubMed: 23452553]
7. Loffroy R, Lin M, Yenokyan G, et al. Intraprocedural C-Arm dual phase cone-beam CT: Can it be used to predict short-term response to TACE with drug-eluting beads in patients with hepatocellular carcinoma? Radiology. 2013;266:636–48. [PubMed: 23143027]
8. Wang X, Erinjeri JP, Jia X, et al. Pattern of retained contrast on immediate postprocedure computed tomography (CT) after particle embolization of liver tumors predicts subsequent treatment response. Cardiovasc Intervent Radiol. 2013;36:1030–8. [PubMed: 23152036]
9. Syha R, Grozinger G, Grosse U, et al. Parenchymal blood volume assessed by c-arm-based computed tomography in immediate posttreatment evaluation of drug-eluting bead transarterial chemoembolization in hepatocellular Carcinoma. Investigative Radiology. 2016;51:121–6. [PubMed: 26488373]
10. Duran R, Sharma K, Dreher MR, et al. A novel inherently radiopaque bead for transarterial embolization to treat liver cancer - A pre-clinical study. Theranostics. 2016;6:28–39. [PubMed: 26722371]
11. Negussie AH, Dreher MR, Johnson CG, et al. Synthesis and characterization of image-able polyvinyl alcohol microspheres for image-guided chemoembolization. J Mater Sci Mater Med. 2015;26:198. [PubMed: 26105830]
12. Ashrafi K, Tang Y, Britton H, et al. Characterization of a novel intrinsically radiopaque drug-eluting bead for image-guided therapy: DC Bead LUMI™. J Control Release. 2017;250:36–47. [PubMed: 28188808]
13. Levy EB, Krishnasamy VP, Lewis AL, et al. First human experience with directly image-able iodinated embolization microbeads. Cardiovasc Intervent Radiol. 2016;39:1177–86. [PubMed: 27206503]
14. Mikhail AS, Pritchard WF, Negussie AH, et al. Mapping drug dose distribution on CT images following transarterial chemoembolization with radiopaque drug-eluting beads in a rabbit tumor model. Radiology. 2018;289:396–404. [PubMed: 30106347]
15. Pritchard WF, Woods DL, Esparza-Trujillo JA, et al. Transarterial chemoembolization in a woodchuck model of hepatocellular carcinoma. J Vasc Interv Radiol. 2020;31:812–9.e1. [PubMed: 32107125]
16. Mauda-Havakuk M, Kassin MT, Mikhail AS, et al. Woodchuck hepatic anatomy and vascular alterations due to hepatocellular carcinoma with angiographic atlas of the abdomen and pelvis. J Vasc Interv Radiol. 2021.
17. Wilkins LR, Stone JR, Mata J, et al. The use of the woodchuck as an animal model for evaluation of transarterial embolization. J Vasc Interv Radiol. 2017;28:1467–71. [PubMed: 28941521]
18. Kim AY, Yacoub JH, Field DH, et al. Suitability of the woodchuck HCC as a preclinical model for evaluation of intra-arterial therapies. Animal Model Exp Med. 2020;3:98–102. [PubMed: 32318666]
19. Jacob JR, Sterczer A, Toshkov IA, et al. Integration of woodchuck hepatitis and N-myc rearrangement determine size and histologic grade of hepatic tumors. Hepatology. 2004;39:1008–16. [PubMed: 15057905]
20. Mikhail AS, Mauda-Havakuk M, Partanen A, et al. Liver-specific 3D sectioning molds for correlating in vivo CT and MRI with tumor histopathology in woodchucks (Marmota monax). PLoS One. 2020;15:e0230794. [PubMed: 32214365]
21. Thompson JG, van der Sterren W, Bakhutashvili I, et al. Distribution and Detection of Radiopaque Beads after Hepatic Transarterial Embolization in Swine: Cone-Beam CT versus MicroCT. J Vasc Interv Radiol. 2018;29:568–74. [PubMed: 29500000]

22. Dreher MR, Sharma KV, Woods DL, et al. Radiopaque drug-eluting beads for transcatheter embolotherapy: experimental study of drug penetration and coverage in swine. J Vasc Interv Radiol. 2012;23:257–64. [PubMed: 22178039]

23. Namur J, Citron SJ, Sellers MT, et al. Embolization of hepatocellular carcinoma with drug-eluting beads: doxorubicin tissue concentration and distribution in patient liver explants. J Hepatol. 2011;55:1332–8. [PubMed: 21703190]

24. Gaba RC, Baumgarten S, Omene BO, et al. Ethiodized oil uptake does not predict doxorubicin drug delivery after chemoembolization in VX2 liver tumors. J Vasc Interv Radiol. 2012;23:265–73. [PubMed: 22178040]

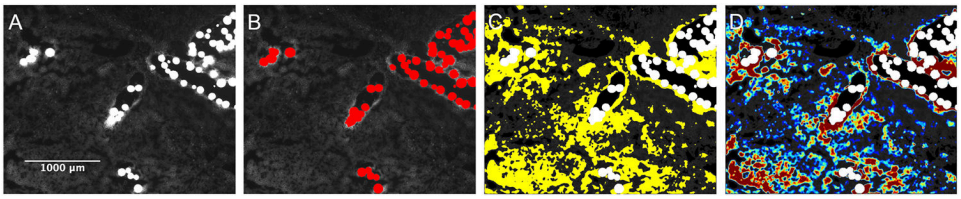

Figure 1.

Image segmentation and generation of doxorubicin extravascular heatmaps. A) Fluorescence microscopy image of radiopaque DEB in woodchuck HCC. B) Segmentation of DEB mask (pseudo-colored red). C) Segmentation of doxorubicin in extravascular tumor compartment (pseudo-colored yellow). D) Pseudo-colored heatmap depicting concentrations of eluted doxorubicin. Red represents the highest concentration and blue represents the lowest concentration.

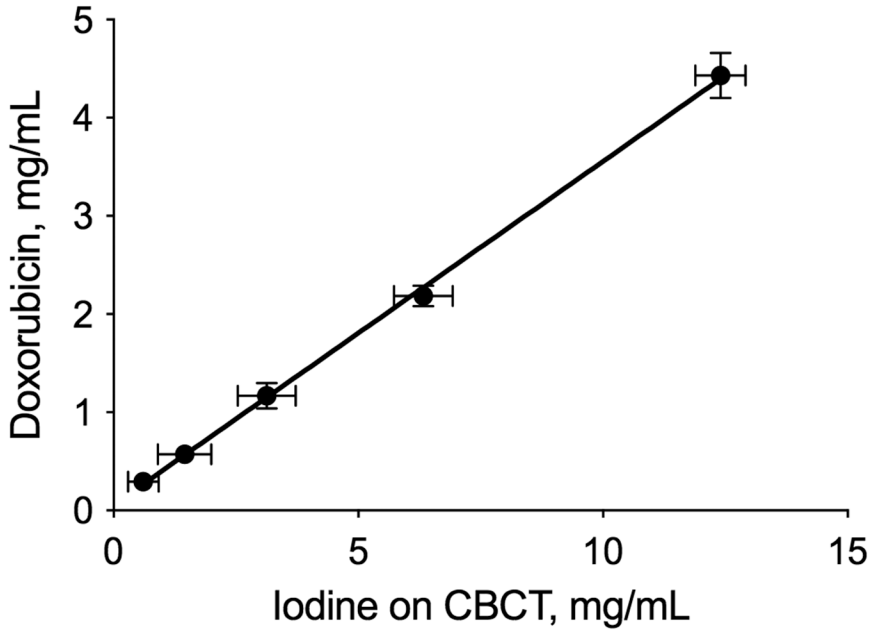

Figure 2.
Correlation between doxorubicin measured in DEB phantoms and iodine measured on cone-beam CT. Plot of doxorubicin measured in 1 mL phantoms containing a range of DEB densities (0.78-12.5% (v/v)) vs iodine measured on cone-beam CT (100 kVp).

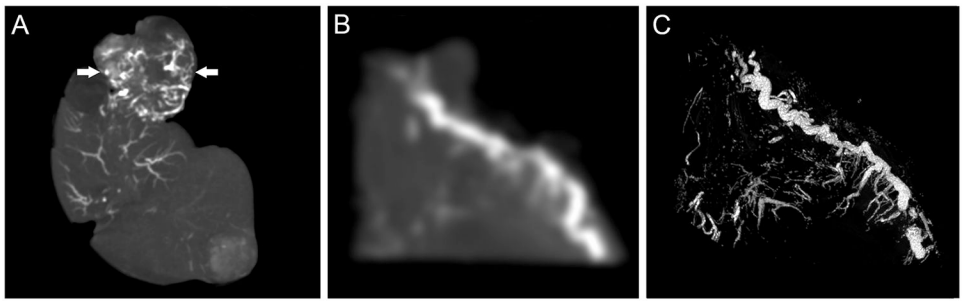

Figure 3.

Imaging of radiopaque DEB in embolized tumor and tissue samples. A) Cone-beam CT of liver explant showing radiopaque DEB in the liver and tumor (arrows) blood vessels. B) Cone-beam CT maximum intensity projection (MIP) and C) microCT MIP of the same 5 mm thick tumor sample sectioned using a 3D cutting mold.

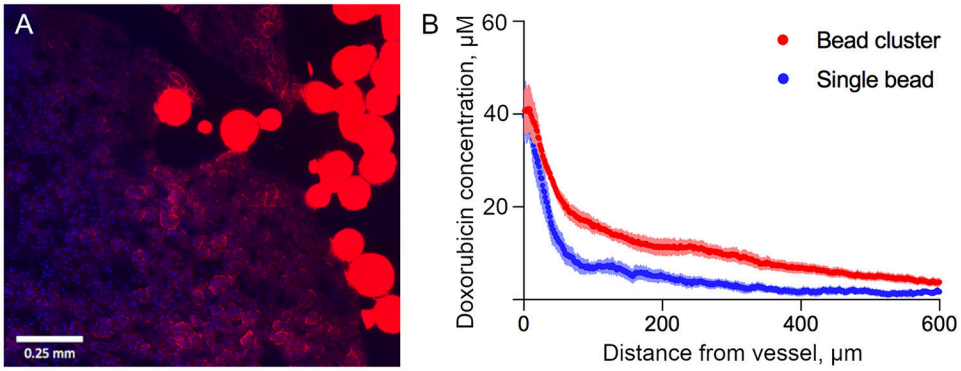

Figure 4.

Extravascular penetration of doxorubicin. A) Fluorescence image showing partial elution of doxorubicin (red) from DEB into extravascular tumor tissue (blue nuclei) 45 minutes after embolization. B) Radial penetration profiles of doxorubicin eluted from single DEB and DEB clusters located in tumor blood vessels. The error bars represent standard error of the mean.

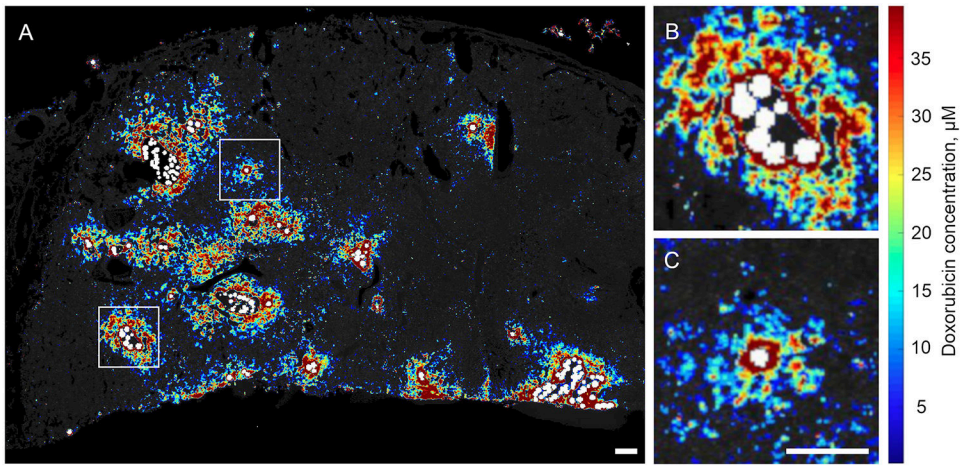

Figure 5.

Doxorubicin "heatmap" of tumor section showing drug concentration gradients (red = higher doxorubicin concentrations, and blue = lower doxorubicin concentrations) surrounding vessels containing DEB (pseudo-colored white). A) Heterogeneous intratumoral distribution of variably sized DEB clusters. Higher doxorubicin concentrations were apparent adjacent to blood vessels containing DEB clusters (B) compared to single DEB (C). Inlays are digital magnifications of the regions within the white boxes in A). Scale bars are 0.5 mm. B and C are the same scale.

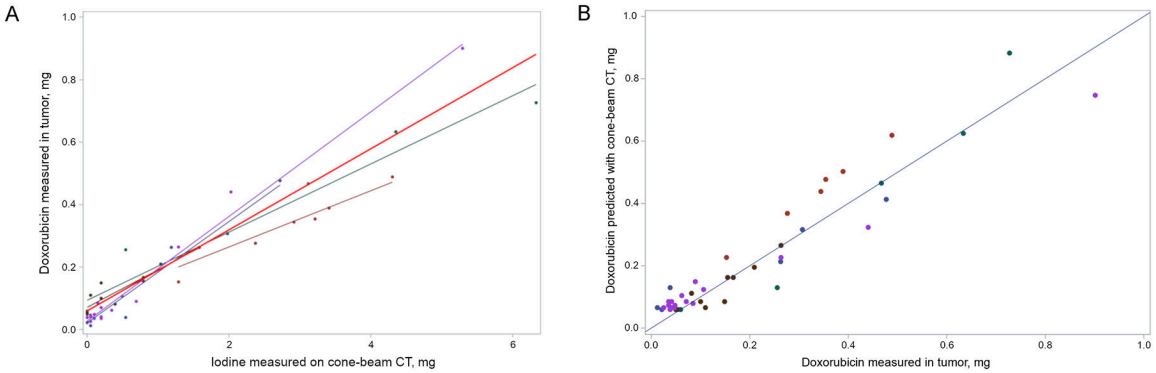

Figure 6.

Correlation and prediction of doxorubicin in tumor samples with iodine measured on cone-beam CT. A) Regression of doxorubicin measured in tumor samples versus iodine measured on cone-beam CT. Each color represents samples from an individual woodchuck. The red line represents the overall regression line using data from all five woodchucks. (B) Comparison of doxorubicin measured in tumor samples to doxorubicin predicted based on models correlating iodine measured on cone-beam CT and doxorubicin measured in tumor sections that were not included in model development. The 1:1 line is shown as a benchmark.

Table 1.

Analyses of model predictions of doxorubicin content in liver tumors based on iodine measured on cone-beam CT scans of HCC samples.

Predictor	Number of woodchucks in model	Correlation	Residuals (actual - predicted)					
			Average	Median	Min.	Max.	RMSE*	AAR†
Iodine (mg)	5	0.956	−0.0173	−0.0184	−0.1549	0.1544	0.0658	0.0494
	4‡		−0.0214	−0.0223	−0.1920	0.2064	0.0812	0.0595

Residuals are calculated based on the "overall line"

*RMSE = Root Mean Squared Error = √(Uncorrected Sum of Squares / N)

†AAR = Average of absolute value of residuals

‡The model with 4 woodchucks is run 5 times, each time with 1 woodchuck excluded, the one for which doxorubicin is predicted